Geothermal point sources identified in a fumarolic ice cave on Erebus volcano, Antarctica using fiber optic distributed temperature sensing

Aaron Curtis[1] and Philip Kyle[1]

Received 27 May 2011; revised 11 July 2011; accepted 12 July 2011; published 17 August 2011.

[1] Degassing of CO_2 on the flanks of the active Erebus volcano is thought to occur mainly through fumarolic ice caves (FIC) and associated fumarolic ice towers. There is also minor CO_2 degassing from isolated areas of warm ground. The mechanism supplying heat and CO_2 gas into the FIC is poorly understood. To investigate this system, a fiber optic distributed temperature sensing (DTS) system was deployed in a FIC to obtain temperature measurements every meter. The DTS data reveal that localized gas vents (GV) supply heat to the FIC air mass and are an important component of the FIC microclimate. FIC temperature is anti-correlated with local atmospheric pressure, indicating barometric pumping of the GV. These results enable the use of FIC temperature as a proxy for flank degassing rate on Erebus, and represent the first application of DTS for monitoring an active volcano.
Citation: Curtis, A., and P. Kyle (2011), Geothermal point sources identified in a fumarolic ice cave on Erebus volcano, Antarctica using fiber optic distributed temperature sensing, *Geophys. Res. Lett.*, *38*, L16802, doi:10.1029/2011GL048272.

1. Introduction

[2] Fumarolic ice caves (FIC) in the summit caldera of the active Erebus volcano are geothermal features which permit a unique opportunity to quantify and understand volcanic flank degassing, and may also serve as important analogues for extraterrestrial phenomena. FIC are networks of passages melted into the base of the snowpack, where geothermal heat and warm gases are supplied to the ice-rock interface. Permafrost and ice cover typically seals the bedrock surface of Erebus to gas release except at the entrances of FIC. Conical towers of ice up to 10m tall, known as fumarolic ice towers, form over many of the FIC entrances. There are over a 100 FIC in the summit plateau of Erebus volcano (Figure 1). Some additional heat and gas escapes directly through isolated areas of warm ground. *Wardell et al.* [2003] measured CO_2 emissions at 43 entrances and estimated that Erebus releases 0.46 kg s^{-1} of CO_2 from its flanks. Erebus is thus an excellent laboratory for the study of diffuse flank degassing. A better understanding of the dynamics at work in the Erebus FIC can improve management and mitigation at the many volcanic areas around the world where flank degassing is a poorly understood hazard [*D'Alessandro*, 2006]. As structures where warm, vapor-rich gas is channeled through a frozen barrier into a dry, low-pressure (about 600 hPa) environment well below freezing, the FIC systems may share dynamics with the "misty ice caverns" [*Spencer*, 2009] theorized to exist beneath geysers observed emitting H_2O and salts near the south pole of Saturn's moon Enceladus [*Matson et al.*, 2007]. A typical FIC consists of several hundred meters of passage and contains over 1 km^3 of air and volcanic gas.

[3] FIC microclimates are strongly out of equilibrium with the average Erebus surface conditions of −32.9°C and low relative humidity. Air temperatures observed in the FIC are typically around 0°C, relative humidity is 80 to 100%, and CO_2 levels are usually elevated and can be over 2% [*Wardell et al.*, 2003]. *Giggenbach* [1976] attributed the thermal disequilibrium in Camp Cave at Erebus to conductive heat flux through the lava floor. Based on isotherms from 50 temperature points taken at 15 cm depth into the lava regolith he estimated a heat flux of 11.3×10^{-4} J cm^{-2} s^{-1}. We observed that nearly all FIC had discrete gas vents (GV) on their rock floors which emit warm gas (5°C to 25°C). Where GV occur the ceiling of the cave chamber above the vent is often domed due to localized melting. We also observed cold vents (CV) where ambient surface air leaked into the cave.

2. Fiber-Optic Distributed Temperature Sensing (DTS)

[4] To determine the relative importance of the diffuse, conductive heat flux versus the advective flux localized at GV, cave air temperature data with high spatial and temporal resolution was required. Fiber optic distributed temperature sensing (DTS) allows measurement of temperature along a fiber optic cable with spatial resolution as fine as 0.25 m and temporal resolution of 1 Hz. Pioneered by the energy industry, DTS is now an emerging tool in the environmental sciences [*Tyler et al.*, 2009], particularly hydrology [*Selker et al.*, 2006]. A recent investigation in Carlsbad Caverns pioneered the use of DTS in a limestone cave [*Dwivedi*, 2010], but the technology has yet to be applied to ice caves, glacier caves, or lava tubes. Thus far geothermal applications of DTS had been limited to well monitoring [e.g., *Ouyang and Belanger*, 2006], and it had not yet been deployed on an active volcano.

[5] DTS entails sending a laser pulse down a fiber-optic cable and comparing the transmitted spectrum against light returning to the laser source [*Smolen and Van der Speck*, 2003]. Returning light is sourced from scattering at the fiber's core-cladding boundary, which occurs along the entire length of the cable. The return spectrum contains useful wavelength peaks in addition to the primary peak (which is the incident wavelength). Raman-spectrum DTS studies such as ours obtain a temperature value by comparing the

[1]Department of Earth and Environmental Science, New Mexico Institute of Mining and Technology, Socorro, New Mexico, USA.

0094-8276/11/2011GL048272

two wavelength peaks resulting from inelastic scattering: the Stokes and anti-Stokes bands. The prevalence of anti-Stokes scattering events is highly dependent on temperature, compared to the Stokes scattering events which are only slightly affected by temperature. As a result, the ratio between the Stokes and anti-Stokes band peak intensities is proportional to temperature.

3. Methods

[6] In this study we examine the temperature distribution in Warren cave, a passage system with one simple entrance (no ice tower). We deployed 438 m of double stranded Infinicor SXi 50/125 micrometer optical fiber in a tight buffer cable with an Aramid strength member in a loop extending to the back of the cave (Figure 2g). The cable was suspended from poles so that it was not affected directly by conduction from the rock but instead measured the adjacent cave air temperature. The cable was over 50 cm from rock and ice except in two passages <1 m in diameter.

[7] A conventional survey was made of Warren cave in the 2009–2010 Austral summer field seasons and a LiDAR survey in 2010–2011. These combined with a survey of the cable location gave a 3-dimensional location for each temperature point in the cave. Fiber length was verified using an air-activated chemical hand warmer pack tied to the cable at 397 m. Both ends of the cable terminated near the cave entrance. The cable's two fiber strands were spliced together at the "far end" in a plastic turnaround box. At the "near end," the two fibers were each connected to one channel of a Sensornet Oryx DTS system using E2000 connectors. In this configuration, the laser pulse is sent along the entire length of the fiber in alternating directions. This double-ended method allows correction for differential loss of the Stokes and anti-Stokes signals which occurs with distance along the fiber optic cable.

[8] Temperatures were calibrated using warm and cold calibration baths. Absolute temperatures of each were continuously recorded with a NIST-certified platinum resistance thermistor. The cold bath was a bucket filled with a slush of snow with a small amount of water to maintain near-freezing temperatures. The warm bath was a box of sand placed in a GV to maintain a temperature near the upper limit encountered in Warren Cave. Both baths contained 15m of coiled fiber-optic cable.

[9] The DTS was programmed to collect a temperature trace every 10 minutes. Each measurement cycle consisted of firing laser pulses for 15 seconds from the forward channel, followed by 15 seconds of pulses from the reverse channel, and a standby period. Average Stokes and anti-Stokes intensities from the 15 second periods were recorded into onboard memory and processed into temperature using Sensornet software. Using the time of flight based on the constant speed of light in the fiber, the DTS split the return signal into segments corresponding to 1.01m intervals along the fiber.

4. Results

[10] About 0.5 million temperature points were recorded in Warren cave between 6:10 (UTC) on 16 December 2010 and 15:30 on 26 December 2010. The DTS temperatures were converted to absolute temperatures using a linear least-squares regression between the PT100 and DTS calibration bath measurements (Figure 3). The resulting dataset is shown in Figure 2a. The temperature values have a resolution better than ±0.13°C calculated using the standard deviation of temperatures from the calibration baths [*Smolen and Van der Speck*, 2003]. This value assumes the calibration baths to be precisely the same temperature throughout. In reality there is some degree of thermal heterogeneity and stratification in the sand and ice/water slush and therefore the actual resolution is probably closer to the manufacturer's estimated value of 0.05°C.

[11] Location of the DTS cable is shown in Figure 2g. Before and during cable installation, GV and CV locations were recorded. Three gas vents, GV2 (at 630 m along the fiber cable), GV4 (670 m), and GV5 (705 m), are marked by time-averaged temperature anomalies of greater than 1°C (Figure 2c). GV1, at 299m, is marked by a less conspicuous temperature anomaly of 0.3°C. The two CV are each associated with a −3°C temperature anomaly. The CV2 anomaly appears at 260m, and CV1 is at both 137m and 377m because the cable passes through that area (Ostrich hall) twice. Our distance verification hand warmer caused a temperature spike from 1.2 to 2.4°C, which relaxed to background after about 24 hours.

[12] Spatially averaged cave temperature (T_c) varied from 0.1 to 1.3°C during the DTS campaign. Two periods of low temperatures can be identified: Dec 17 to 19 and Dec 21 to 24. These cold excursions are also present in the GV and CV temperatures, but with a range of amplitudes below and above the amplitude of the cave average. The relative amplitude of temporal variation is reflected in the width of the confidence intervals. Figure 2b shows temperatures averaged over time for each virtual thermometer, with confidence intervals based on 2ó of all data from that virtual thermometer. Temperature, windspeed and pressure records from the Lower Erebus Hut weather station, located 1.0 km northwest of the Warren cave entrance, are shown in Figures 2d and 2e for comparison with the cave data.

5. Analysis

[13] There is a strong negative correlation between spatially averaged cave temperature (T_c) in Warren cave and barometric pressure at the Lower Erebus Hut (Figures 2b and 2d). A linear least-squares regression of T_c versus air pressure has an adjusted r^2 of 0.66 (Figure 4). There is no correlation between T_c and air temperature or windspeed, so storms can be ruled out as a driver of cave temperature change and the relationship between barometric pressure and T_c must be direct. A similar effect was observed at Mammoth Mountain, California by *Rogie et al.* [2001], in which changes in barometric pressure affected the flux of diffuse soil CO_2 emissions. At Mammoth Mountain, soil CO_2 concentration was effectively a proxy for soil gas flux. The temperatures measured at Warren cave are likewise a proxy for gas flux into the FIC. A time series of CO_2 concentration data from GV in Warren Cave are currently being collected to confirm the assumption that temperature can be used as a proxy for FIC gas flux. Both systems probably share a physical mechanism: a pressure head is set up in response to pressure imbalance between the atmosphere and the gas volume in the volcanic edifice, and gas flux occurs in proportion to that head. At Mammoth Mountain, spatially distributed soil

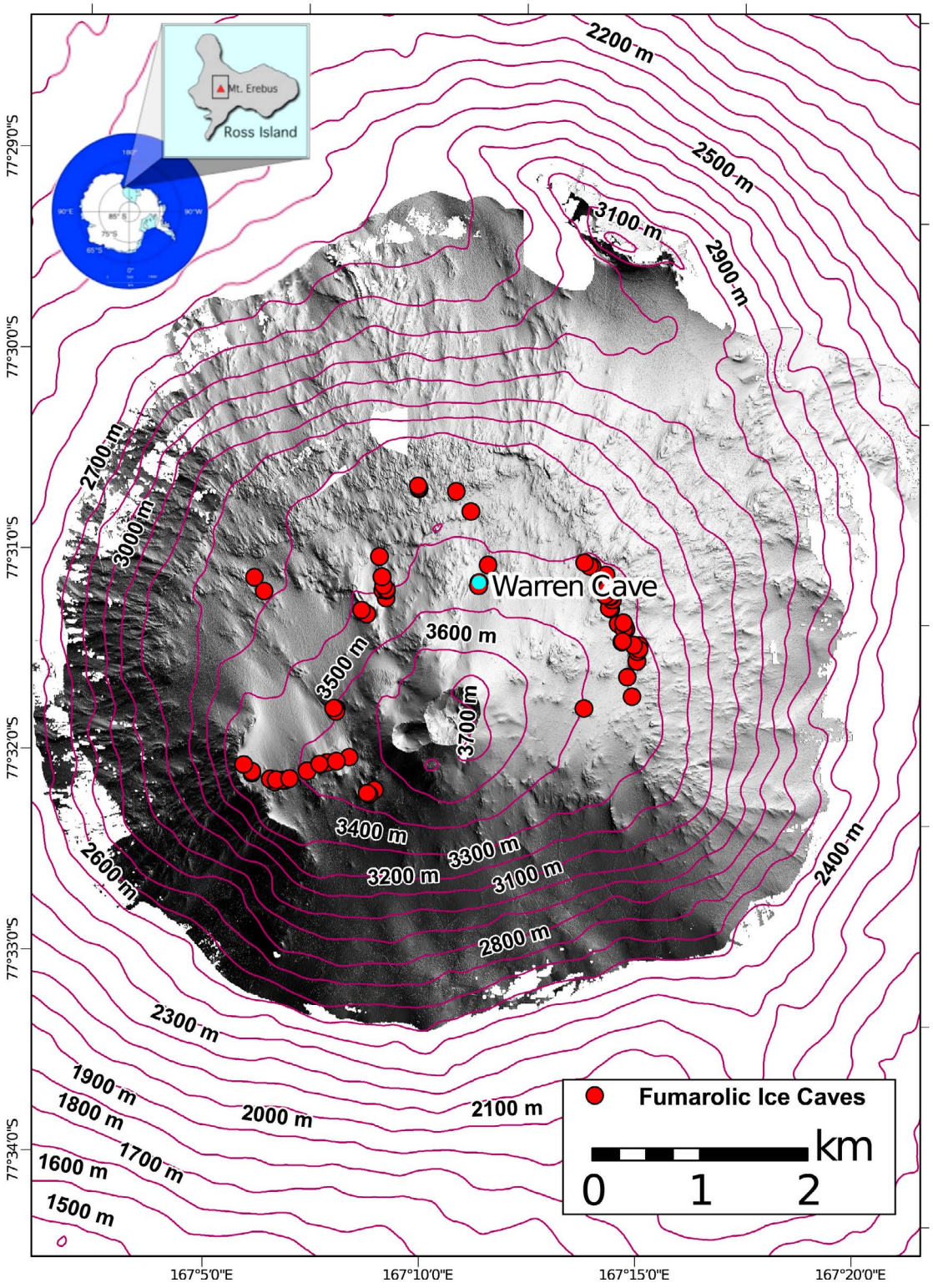

Figure 1. Location map of the study area.

CO_2 measurements revealed diffuse gas release over 2 km^2, but within that area there were at least five point sources where gas flux was more than 40 times greater than the average gas flux. Those areas are comparable to the GV in Warren Cave.

[14] The relationship between barometric pressure and T_c exhibits hysteresis (Figure 4). During periods of decreasing pressure (green circles), the temperature/pressure relationship has a steeper slope then during periods of increasing pressure (blue circles). Physically, this indicates that the

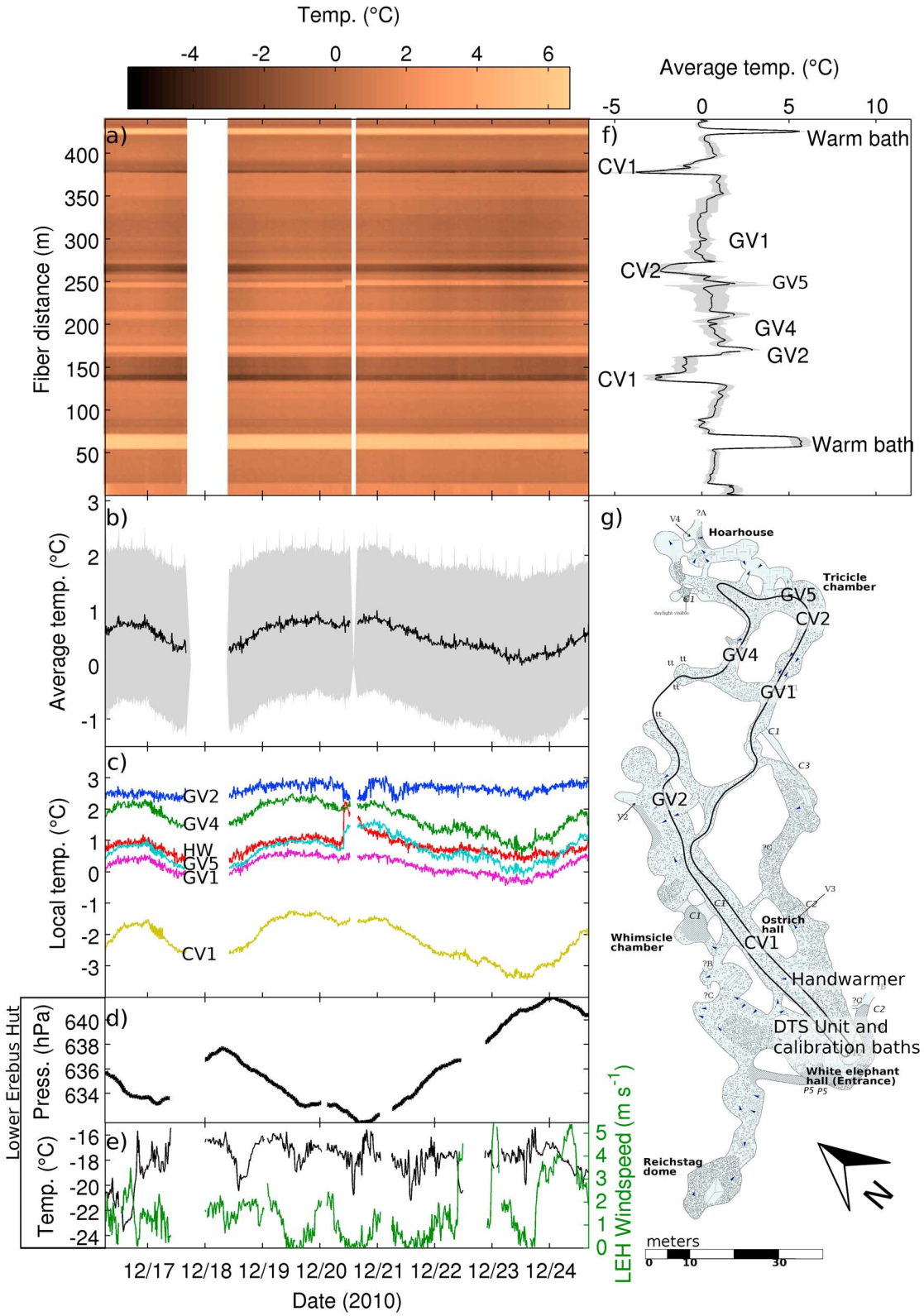

Figure 2. (a) DTS results, after linear correction per Figure 1. (b) Warren cave temperature averaged over space, plotted with an area representing 1σ above and below the data. The large standard deviation represents the spatial variability throughout the cave. (c) Temperatures from selected locations in the cave. GV are warm gas vents, CV are cold tubes admitting external air into the cave. (d) Barometric pressure recorded at the Lower Erebus Hut weather station. (e) Temperature (blue) and windspeed (green) recorded at the same station. (f) Warren cave temperature averaged over time, plotted with an area representing 2σ above and below the data. (g) Conventional cave map of Warren Cave completed during the 2009–2010 field season. The thick black line represents the DTS cable location, and GV and CV are labeled.

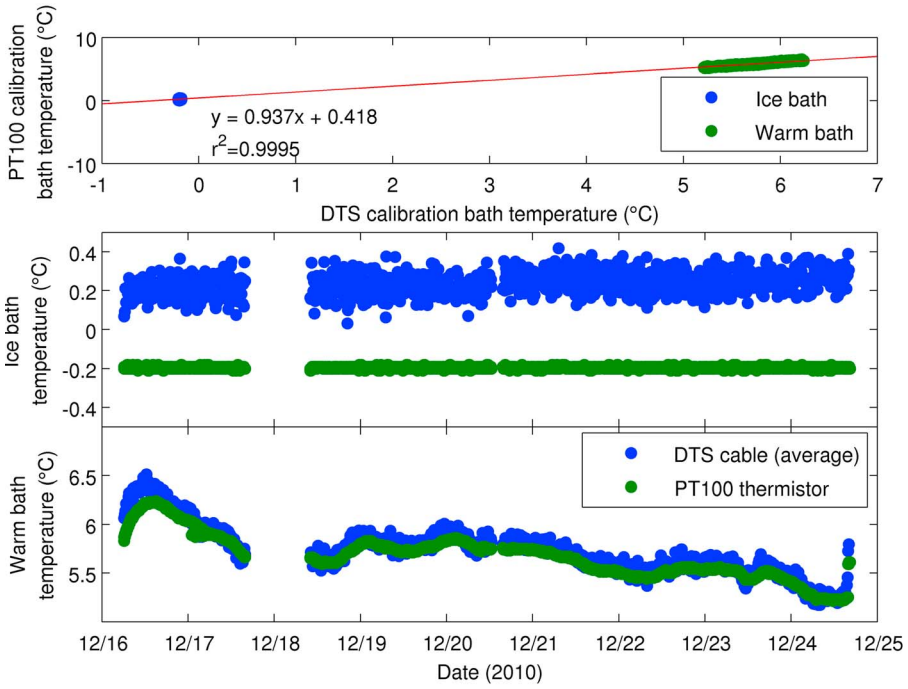

Figure 3. Correction of DTS temperatures using NIST-certified PT100 thermistors in the warm bath (a box of sand in a vent) and cold bath (a bucket containing a snow/water mix at equilibrium).

"drawing out" of volcanic gas by a pressure drop is a more effective process then the inhibition of gas flow by "pushing in." If the GV and CV are primary sites for gas "draw out," amplitudes of temperature change should be larger at those locations then the amplitude of change in spatially averaged data from the whole cave. GV4, GV5, CV2 all exhibited roughly twice the average cave temperature amplitude, whereas GV1 and GV2 were roughly equal to the average cave amplitude.

[15] Time series of cave temperature at all locations are within 10 minutes (the sampling rate) of being in phase with the cave average. This most likely reflects a well-mixed system due to the strong air flow in the cave. We observed air flow of between 0.5 m s^{-1} and 15 m s^{-1} in passages, consistently flowing towards the entrance from the Tricicle chamber area, which has the lowest elevation is furthest from the entrance. This regime would allow a heat pulse from GV5 in Tricicle chamber to reach the entire cave within a single

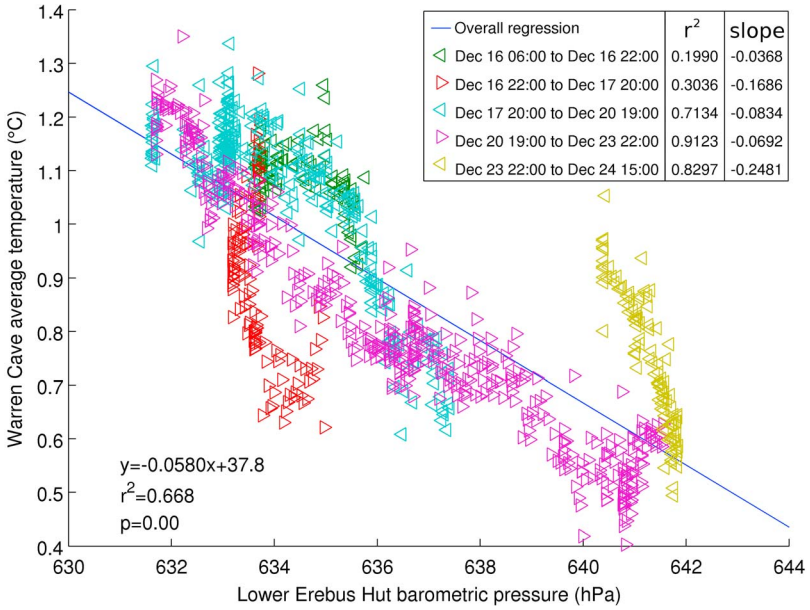

Figure 4. Relationship between average temperature in Warren cave and barometric pressure recorded at the Lower Erebus Hut seismic station. Linear least-squares regression for the whole dataset is shown. Periods of decreasing barometric pressure are plotted as left-pointing triangles, with right-pointing triangles indicating periods of increasing pressure.

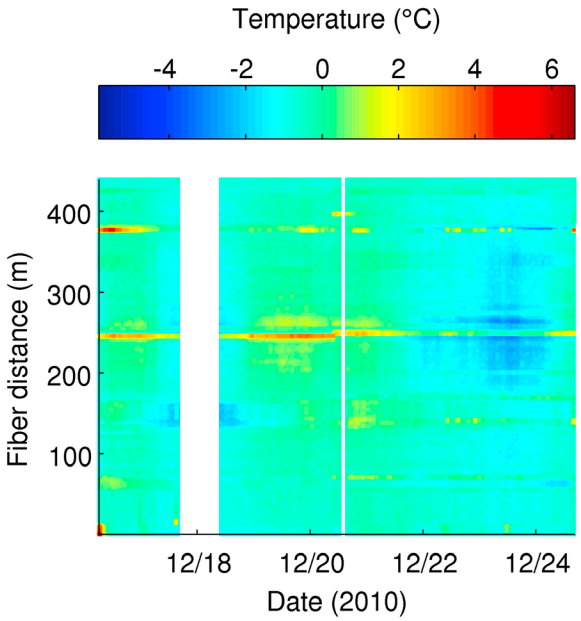

Figure 5. Spatially detrended DTS results, calculated by subtracting the mean for each cable location from the dataset.

sampling period. Synchronization of temperature throughout the cave can be imaged by spatially detrending the data. In Figure 5, the mean of the data obtained at each location has been subtracted from all data for that location. Anomalies visible at 248 m and 375 m are the result of movement in the cable due to redeployment of a section of cable to cover a larger section of the Tricicle chamber area around 10am on 20 Dec and should be ignored. The most significant pattern in the detrended data is that the cold period from 19 to 21 Dec and the warm period from 21 to 24 Dec are stronger at the lower elevations of the cave, furthest from Warren's entrance (center of the plot).

[16] In addition to GV and CV proximity, one explanation for a reduction in temperature variability as the air flows up through the cave towards the entrance involves latent heat associated with sublimation and deposition of ice crystals on the cave walls. Many of the passage walls in Warren cave are covered in large frost crystals which form by direct deposition of water vapor [*Knight*, 1985]. Conversely, liquid water has been observed flowing down melting ice near GV2. Buffering by latent heat has been identified as an important influence on cave air temperatures in European ice caves [*Luetscher*, 2005] and would explain why the majority of air temperature observations in Erebus' FIC are within five degrees of freezing.

6. Conclusions

[17] DTS enabled the identification of thermal point sources, determination of spatially averaged temperatures, and investigation of the spatial synchronicity of temperature change in Warren cave. The instrument and our particular cable configuration performed well despite the challenges inherent in powering and operating such a system in a FIC on an Antarctic volcano. In comparison to transportation, installation, and data management of the over 400 sensors that would constitute an equivalent electronic temperature sensing system, the DTS had a far lower cost, both in terms of money and man-hours. This system is recommended as a component of monitoring campaigns on other active volcanoes around the world. Particularly of interest are volcanoes representing significant hazards and hosting FIC systems including Mt Rainier [*Zimbelman et al.*, 2000] and Mt Baker [*Kiver*, 1978].

[18] Although heat flow to the cave floor surface is primarily conductive [*Giggenbach*, 1976], the high temperature amplitudes and airflows observed at GV demonstrate that localized advection is likely to be a major component of heat transfer from the cave floor to the cave airmass. Advective flux at GV and CV is in turn modulated by barometric pressure. A pressure drop causes a temperature increase throughout the cave, and a pressure increase is associated with temperature drop. These findings lend support to the concept of diffuse degassing in response to barometric pumping and suggest that meteorological observation and prediction could be used to prevent injuries and fatalities such as those that occurred on Etna in 1993 [*D'Alessandro*, 2006] and Mammoth Mountain in 2006 [*Rogie et al.*, 2001].

[19] Over longer timescales, other controls on FIC temperature may be present such as variations in the volcanic geothermal system supplying the GV or changes in the snowpack permeability such as the depth hoar described by *Sokratov and Golubev* [2009]. Further investigation, including a longer DTS time series and installation in a variety of FIC, is required to examine these processes.

[20] **Acknowledgments.** Funding for this project was provided by the NSF Office of Polar Programs through Grant ANT- 0838817 and a NASA Space Grant. DTS hardware and configuration support was supplied by Scott Tyler and Francisco Suarez at the Center for Transformative Environmental Monitoring Programs (CTEMPs). Thanks to Nial Peters, Bill McIntosh, Nelia Dunbar, Matt Zimmerer, Nels Iverson, and Yves Moussallam for assistance in the field, Jevon Harding for fiber splicing lessons, Julian Todd for his open-source cave sketching program Tunnel, and Laura Jones for lidar measurements. Field work was supported by Raytheon Polar Services Company, PHI and Helicopters New Zealand. The manuscript was revised with input from Giovanni Chiodini, Clive Oppenheimer, and an anonymous reviewer.

[21] The Editor thanks Giovanni Chiodini and an anonymous reviewer for their assistance in evaluating this paper.

References

D'Alessandro, W. (2006), Gas hazard: An often neglected natural risk in volcanic areas, in *Geo-environment and Landscape Evolution II*, edited by J. F. Martin-Duque et al., *WIT Trans. Ecol. Environ.*, *89*, 369–378.

Dwivedi, R. (2010), Modeling and field study of cave micrometeorology: Role of natural convection, M.S. thesis, Dep. of Earth and Environ. Sci., N. M. Inst. of Min. and Technol., Socorro.

Giggenbach, W. F. (1976), Geothermal ice caves on Mt Erebus, Ross Island, Antarctica, *N. Z. J. Geol. Geophys.*, *19*(3), 365–372.

Kiver, E. P. (1978), Mount Baker's changing fumaroles, *Ore Bin*, *40*, 133–145.

Knight, C. A. (1985), Growth forms of large frost crystals in the Antarctic, *J. Glaciol.*, *31*(108), 127–135.

Luetscher, M. (2005), Processes in ice caves and their significance for paleoenvironmental reconstructions, Ph.D. thesis, Swiss Inst. for Speleol. and Karst Res., La Chaux-de-Fonds, Switzerland.

Matson, D. L., J. C. Castillo, J. Lunine, and T. V. Johnson (2007), Enceladus' plume: Compositional evidence for a hot interior, *Icarus*, *187*(2), 569–573, doi:10.1016/j.icarus.2006.10.016.

Ouyang, L.-B., and D. Belanger (2006), Flow profiling by Distributed Temperature Sensor (DTS) system—Expectation and reality, *SPE Prod. Oper.*, *21*(2), 269–281.

Rogie, J. D., D. M. Kerrick, M. L. Sorey, G. Chiodini, and D. L. Galloway (2001), Dynamics of carbon dioxide emission at Mammoth Mountain, California, *Earth Planet. Sci. Lett.*, *188*(3–4), 535–541, doi:10.1016/S0012-821X(01)00344-2.

Selker, J. S., L. Thévenaz, H. Huwald, A. Mallet, W. Luxemburg, N. Van De Giesen, M. Stejskal, J. Zeman, M. Westhoff, and M. B. Parlange (2006), Distributed fiber-optic temperature sensing for hydrologic systems, *Water Resour. Res.*, *42*, W12202, doi:10.1029/2006WR005326.

Smolen, J. J., and A. Van der Speck (2003), Distributed temperature sensing—A DTS primer for oil & gas production [online], *Unclassif. Shell Rep. EP2003*, Shell Int., Rijswijk, Netherlands. [Available at http://ctemps.org/pdfs/Shell_DTS_Primer.pdf]

Sokratov, S., and V. Golubev (2009), Snow isotopic content change by sublimation, *J. Glaciol.*, *55*(193), 823–828, doi:10.3189/002214309790152456.

Spencer, J. (2009), Planetary science: Enceladus with a grain of salt, *Nature*, *459*(7250), 1067–1068, doi:10.1038/4591067a.

Tyler, S. W., J. S. Selker, M. B. Hausner, C. E. Hatch, T. Torgersen, C. E. Thodal, and S. G. Schladow (2009), Environmental temperature sensing using Raman spectra DTS fiber-optic methods, *Water Resour. Res.*, *45*, W00D23, doi:10.1029/2008WR007052.

Wardell, L. J., P. R. Kyle, and A. R. Campbell (2003), Carbon dioxide emissions from fumarolic ice towers, Mount Erebus volcano, Antarctica, in *Volcanic Degassing*, edited by C. Oppenheimer, D. M. Pyle, and J. Barclay, *Spec. Publ. Geol. Soc.*, *213*, 231–246.

Zimbelman, D. R., R. O. Rye, and G. P. Landis (2000), Fumaroles in ice caves on the summit of Mount Rainier—Preliminary stable isotope, gas, and geochemical studies, *J. Volcanol. Geotherm. Res.*, *97*(1–4), 457–473, doi:10.1016/S0377-0273(99)00180-8.

A. Curtis and P. Kyle, Department of Earth and Environmental Science, New Mexico Institute of Mining and Technology, 801 Leroy Pl., Socorro, NM 87801, USA. (aarongc@nmt.edu)